Load-aware Nonlinearity Estimation for Elastic Optical Network Resource Optimisation and Management

Rui Wang, Sarvesh Bidkar, Fanchao Meng, Reza Nejabati, Dimitra Simeonidou

***Abstract*—Elastic optical networks have emerged as a promising technology to accommodate high-capacity and dynamic bandwidth demands of next-generation wireless networks. However, similar to the traditional wavelength division multiplexing optical networks, there exists significant challenges to manage nonlinearity effects in elastic optical networks. In this paper, we first analyse state-of-the-art nonlinearity estimation solutions and propose a novel load-aware nonlinearity estimation method. We further present a resource allocation algorithm using the proposed nonlinearity estimation scheme. In case the new embedded lightpath brings additional nonlinearity blocking the existing requests, we propose a mixed integer linear programming model and two heuristic algorithms using the proposed nonlinearity model as the service reconfiguration scheme for efficient resource allocation in elastic optical networks. The objective of the solution is to minimize the spectrum resource usage while satisfying the bandwidth demands of the connection and ensuring the quality of transmission. The proposed solutions are evaluated using an extensive simulation with off-line traffic requests and incrementally loaded requests against the benchmark solutions for two types of traffic profiles in the N6S9 network and the NSF network. The results presented in this paper validate the benefits of the proposed nonlinearity estimation model and the corresponding algorithms to minimize the number of allocated frequency slots and service request blocking ratio while improving the overall network capacity.**

***Index Terms*—Elastic optical networks; fibre nonlinearity estimation; mixed integer linear programming; routing, modulation and spectrum assignment.**

I. Introduction

Elastic optical network (EON) has emerged as a promising technology for backbone networks to meet dynamic, high-bandwidth traffic demands. EON provides better flexibility and service granularity compared to conventional wavelength division multiplexing (WDM) systems by employing flexible spectrum and modulation scheme assignment [1]. However, a more complex control layer mechanism is required to operate EON with finer granularity and more adaptable options. To enable network optimisation in EON, accurate knowledge of physical layer impairments on each link is essential. These impairments directly contribute to the signal-to-noise ratio (SNR) which further influences the system spectral efficiency and capacity. Linear impairments such as chromatic dispersion and polarisation mode dispersion can be compensated by using digital signal processing techniques whereas the nonlinear impairments (NLI) like self-phase modulation, cross-phase modulation and four-wave mixing are difficult to mitigate. NLI is also a key factor that limits the maximum signal power in the fibre which in turn limits the maximum reach distance. Hence, there is a significant need to accurately estimate the NLI to improve the quality of transmission (QoT) assessment of the lightpaths.

Traditionally, the NLI are allocated a certain SNR margin to model their worst-case impact [2]–[4]. Using the SNR margin based on the worst-case impact does not require knowledge of the network, which can significantly reduce the complexity of NLI estimation. In this approach, the maximum transmission distance for each modulation scheme is calculated based on the allocated margins for NLI and other impairments to guarantee error-free transmission. This method also enables distance adaptive routing, spectrum and modulation assignment (RMSA) in EON. Various RMSA solutions have been proposed in [5]–[11] to improve network resource utilization of the EON. In these solutions, the maximum transmission distance possible for each modulation format is dependent on the margins allocated to different noise components (e.g. fibre aging/breaking, transponder aging, NLI). However, the margin for NLI is calculated assuming fully loaded channel and worst-case nonlinear impairments, without considering the signal transmission power, routing and spectrum allocation. Using maximum transmission distance method results in the overestimation of the NLI. Therefore, some lightpaths adopt conservative modulation formats which reduces the spectral efficiency and hence underutilizing the optical network resources. Also, assuming a high margin for NLI often requires more powerful transceivers and more regenerators to be deployed in the network which further leads to an increase in the capital expenditure.

A significant amount of research has been carried out for RMSA problem to improve optical network efficiency by modelling physical layer impairments. Network kriging and norm minimization techniques are used in [12] to model the impact of NLI for lightpaths and used for regenerator placement. Due to the simplification, it lacks accuracies by assigning a margin for NLI from distant channels. NLI has been modelled in optical OFDM systems for lightpath QoT assessment in [13]. However, it only considers FWM, leading to underestimation of the NLI. The Gaussian noise (GN) model [14], [15] has been proposed to model the effect of nonlinear impairments occurred during transmission. In

[16]–[19], integer linear programming (ILP) formulations have been proposed to address the nonlinearity-aware RMSA problem in EON based on simplified GN model. Similarly, heuristic RMSA algorithms considering NLI are proposed in [19]–[21]. The NLI models in [16]–[19] only consider the self-channel interference and the cross-channel interference but ignore the multi-channel interference. Due to this limitation, each connection requires at least 28 GHz bandwidth to precisely capture the NLI. For the channel occupying less than 28 GHz, these models underestimate the NLI significantly which may lead to lightpaths setup failure at planning stage. These papers do not consider online traffic requests which fail to meet the dynamic demand of future services. In [22] [23], it shows that using exact NLI results in serious inter channel blocking problem, as future lightpaths introduce more NLIs to existing lightpaths using the same links. The excess NLI may lead to QoT of some lightpaths degrading below the SNR threshold for the particular assigned modulation format. The connections are blocked as error-free transmission is no longer guaranteed. In [20] [21], the central channel NLI power spectral density (PSD) is calculated based on GN model assuming fully occupied C-band (worst-case NLI) and then the NLI PSD is used for the RMSA algorithm regardless of the spectrum assignment. This approach is similar to maximum transmission distance method, which results in NLI overestimation.

Based on the existing literature review, to the best of our knowledge, there is no tool for a fast and accurate NLI estimation to provision dynamic incrementally loaded connection requests. Therefore, we first propose a fast NLI estimation model based on GN model [14] [24] for RMSA problem in EON. We extend our previous work in [25] by proposing a complete algorithm to provide RMSA solution in the service incrementally loaded EON, with several service reconfiguration schemes to reconfigure the existing service requests in case that NLI of future service blocks the existing service connections. The reconfiguration schemes include: 1) a comprehensive mixed integer linear programming (MILP) formulation; 2) a MILP based heuristic reconfiguration algorithm and 3) a complete heuristic reconfiguration method. We first compare the performance of the 3 proposed service reconfiguration schemes with benchmark methods for two topologies and various signal PSDs. The performance of the complete RMSA algorithm with reconfiguration algorithms is then evaluated and results are presented. The paper is organized as follows: Section II explains our proposed hybrid nonlinearity estimation model. Section III discusses the accuracy of the proposed NLI model. Section IV present the heuristic main algorithm and the proposed service reconfiguration schemes. In Section V, we explain the network simulation setup, the benchmark method and present the results and Section VI concludes the paper.

II. Physical Layer Impairments Model

In this section, we first explain the physical layer impairment model and various assumptions in this paper. We assume: 1) a transparent dual-polarisation (DP) optical system using coherent detection without in-line compensation; 2) all optical nodes are bandwidth-variable spectrum selective switches with colorless directionless and contentionless capability; 3) polarisation dependent loss is not considered; 4) polarisation mode dispersion and chromatic dispersion are fully compensated using digital signal processing technique; 5) signal spectrum close to rectangular, without guard band between channels; 6) nonlinearity accumulates incoherently; 7) node insertion loss is not considered; 8) equal signal PSD among channels within the same fibre link; 9) power loss is completely compensated by the erbium doped fibre amplifiers (EDFA) of each span; 10) the optical system is deployed with tunable, bandwidth variable and modulation level adaptable transponders; 11) fibre spans are of equal length; 12) the bandwidth request includes the capacity for forward error correction (FEC) overhead.

We consider the amplified spontaneous emission (ASE) noise and NLI as dominant penalties in the uncompensated optical network. The SNR at the receiver is calculated as:

$$SNR_{Rx} = \left(\sum_{l} \frac{1}{SNR_l}\right)^{-1} \quad (1)$$

where the SNR_l is the linear SNR of link l. The end-to-end linear SNR SNR_{Rx} depends on the linear SNR degradation of each link along the path. The linear SNR of each link is calculated as:

$$SNR_l = G^l_{sig}/(G^l_{ASE} + G^l_{NLI}) \quad (2)$$

where G^l_{sig}, G^l_{ASE} and G^l_{NLI} are the PSD for the signal, ASE noise and the NLI of link l within the channel respectively. Since we assume the signal power loss can be fully compensated by EDFA placed between fibre spans, the single sided PSD of ASE noise per span is expressed as [26], [27]:

$$G_{ASE} = 10^{\frac{NF}{10}} \cdot h\nu (10^{\frac{A_e}{10}} - 1) \quad (3)$$

where NF is the noise figure of EDFA, h is Planck's constant, ν is signal carrier frequency and A_e stands for signal power loss over fibre span e in dB.

Compared to the simple model of ASE, NLI such as SPM, XPM and FWM in optical fibre have complex models [28]. To overcome the limitations of aforementioned NLI models, we propose a hybrid NLI model based on GN model for RMSA problem in EON. In hybrid NLI model, few concepts are introduced first. C continuous frequency slots are defined as a spectra window (window size: $C \cdot b$, b is the per frequency slot bandwidth). For a network with F frequency slots, there exists F/C windows. We set $LS = F/C$ representing the windows number, also known as the link loading states number. Then we define the loading state of a link as:

$$ls = \begin{cases} \left\lceil \frac{MF}{F} \cdot LS + \frac{1}{\mu} \right\rceil, & MF < F \\ LS, & MF = F \end{cases} \quad (4)$$

where MF is the maximum slot index among the allocated frequency slots of the link, μ is a very large number and $\lceil\ \rceil$ is a ceiling function giving the smallest integer greater than the input as the output. Factor μ ensures the link loading states to be 1 (minimum) when no slot is assigned. By defining LS loading states, the spectrum occupation of the link can be divided to LS states. As defined in (4), the link is of ls loading state when its maximum allocated frequency slot index MF is within range from $C \cdot (ls - 1)$ *to* $C \cdot ls - 1$ (except $MF = F$). Fig. 1 shows an example of two link loading states. In this example, we consider 1 THz bandwidth with each slot width being 12.5 GHz, spectra window size is 100 GHz, and $LS = 10$. The red block stands for the actual slot allocation of the link. The maximum index of the allocated slot in Fig. 1 (a) is 7, thus the loading state is 1 according to (4). Fig. 1 (b) shows that the link loading state is 2 as the maximum actual occupied slot index is 13.

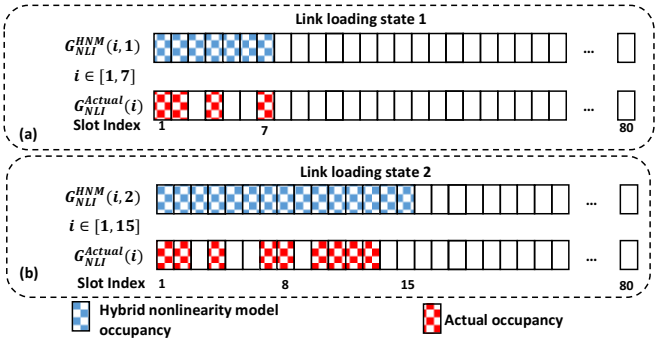

Fig. 1: An example of link loading states. (a) link of loading state 1; (b) link of loading state 2.

As the NLI is related to the spectrum assignment, the proposed hybrid NLI model is limited to using first-fit assignment due to the definition of link loading state in this work. First-fit spectrum allocation is adopted as it is shown as one of the best schemes to achieve minimum blocking probability [29]. Considering the first-fit spectrum assignment, the loading state of a link reflects its loading condition. With higher loading states of a link, the link becomes more congested, resulting in higher NLI noise of all the channels propagating through the link. Therefore, ls is a key factor determining the NLI of the channels. As the NLI PSD does not fluctuate significantly within small bandwidth [14], [30], we choose the NLI PSD of the central frequency of a frequency slot as the NLI PSD for the slot. The single-span NLI PSD of each slot is calculated in advance for all link loading states ($ls^* = 1 \dots LS$) assuming the full occupation of ls^* spectra windows from first frequency slot index to the last index $\frac{F}{LS}\cdot ls^* - 1$ (except when the $MF = F$, $ls = LS$), as shown:

$$G_{NLI}(i\cdot b, ls^*) = \frac{16}{27}\gamma^2 L_{eff}^2 \qquad if\ MF < F$$
$$\int_0^{(\frac{F\cdot ls^*}{LS}-1)\cdot b}\int_0^{(\frac{F\cdot ls^*}{LS}-1)\cdot b} G_{sig}(f_1)\cdot G_{sig}(f_2)\cdot G_{sig}(f_1+f_2 - i\cdot b)\cdot\rho(f_1,f_2,i\cdot b)df_1\, df_2 \qquad (5.1)$$

$$G_{NLI}(i\cdot b, ls^*) = \frac{16}{27}\gamma^2 L_{eff}^2 \qquad if\ MF = F$$
$$\int_0^{B}\int_0^{B} G_{sig}(f_1)\cdot G_{sig}(f_2)\cdot G_{sig}(f_1+f_2 - i\cdot b)\cdot\rho(f_1,f_2,i\cdot b)df_1\, df_2 \qquad (5.2)$$

where i is the frequency slot index ($i \in (1 \dots \frac{F}{LS}\cdot ls^* - 1)$ if $MF < F$, otherwise $i \in (1 \dots F)$) and B is the total bandwidth which equals to $F \cdot b$, ρ denotes a normalized factor depending on the type of amplifier between spans. In Fig. 1 (a) and (b), the blue block represents the how the NLI is calculated using the proposed hybrid nonlinearity model assuming slot 1 to $F{\cdot}ls/LS - 1$ fully occupied as depicted in (5.1) or 1 to F for (5.2). We assign the NLI value calculated from the hybrid NLI model (blue blocks) to the actual allocated slots (red blocks) in the link according to their index i and the link loading state ls^*. The assigned hybrid NLI value is always larger than or equal to the exact NLI value as the hybrid NLI model is the worst-case NLI for each link loading state. In case the slots are assigned in the way shown as the red block in Fig. 1 (b), the link is within loading state 2. Therefore, we assign the pre-calculated $G_{NLI}^{HNM}(8,2)$ to the slot 8 as its NLI PSD rather than calculating the exact NLI PSD $G_{NLI}^{Actual}(8,2)$. In this case, the $G_{NLI}^{HNM}(8,2)$ is always greater than or equal to the actual NLI PSD $G_{NLI}^{Actual}(8,2)$ regardless of the spectrum assignment as long as the link loading state is 2.

The hybrid NLI model combines the features of worst-case NLI method due to full slots occupation within spectra windows of each loading state and the greedy exact NLI estimation strategy as it considers the channel loading conditions. This approach creates a lookup table for NLI according to the link loading state ls^* and the frequency slots indexes assigned to the lightpath. Due to rectangular spectra shape, we formulate the hybrid NLI lookup table by combining (5.1) and (5.2) to form (6), written as:

$$G_{NLI}(i, ls^*) = G_{sig}^3 \cdot \chi_{i,ls^*} \qquad (6)$$

where χ_{i,ls^*} is the NLI PSD coefficient (unit: THz^2/mW^2) of slot index i when the link is of ls^* loading state. ls^*present the particular loading state of the link while the ls is a variable ranging from 1 to LS. The factor χ_{i,ls^*} is the integral results from (5.1) and (5.2) without the G_{sig}, which is similar to nonlinear coefficient in [14]. The optimal signal PSD of a link within ls^* loading state can be expressed as:

$$G_{sig} = \sqrt[3]{G_{ASE}/(2\cdot max(\chi_{i,ls^*}))} \qquad (7)$$

where the function max takes the maximum value of the NLI PSD coefficients of ls^* loading state. The signal PSD in (7) is the differential results of combining (2) and (6), aiming to maximize the SNR of central slot of ls^* loading state.

As the NLI of different loading states are calculated based on given fibre parameters and signal PSD, the model in (5.1) and (5.2) is more accurate than assigning SNR margins for NLI or the worst-case NLI. As the proposed hybrid NLI model is a step-wise model with links are associated with loading states, the nonlinearity is always slightly overestimated when the link remains in the same loading state. Since the proposed hybrid NLI model is based on original GN model, NLI estimation can be applied to channel with less than 28 GHz bandwidth. In EON, the NLI PSD is frequency dependent. Therefore, for a channel occupying multiple frequency slots, NLI PSD is computed by averaging the NLI PSD of the assigned slots as:

$$G_{NLI}^{span,l} = \sum_{i=FS_{min}}^{FS_{max}} G_{NLI}(i, ls^*)/(FS_{max} - FS_{min}+1) \qquad (8)$$

where $G_{NLI}^{span,l}$ is the single span NLI PSD for the channel of the link l in loading state ls^*, FS_{min} and FS_{max} is the minimum and maximum frequency slot index. Combing the NLI from each span, the NLI PSD of link l is expressed as:

$$G_{NLI}^{l} = \sum_{span=1}^{SP_l} G_{NLI}^{span,l} \qquad (9)$$

where the SP_l stands for spans number of the link l. By combining (1) – (3) and (5) – (9), we can calculate the end-to-end SNR to form the QoT evaluation, which is utilized in the following proposed RMSA solutions.

III. Accuracy of Proposed Hybrid Nonlinearity Model

In this section, we analyse the accuracy of the proposed hybrid NLI model by comparing it with exact NLI using original GN model in [14]. The spectra window size is set to be 100 GHz (12.5 GHz per slot), thus the number of loading states LS is 10 for the link gradually loaded from 0 to 1 THz. Therefore, there are $8{\cdot}i$ slots evaluated for link loading state i. Single mode fibre with loss coefficient of 0.22 dB/km, fibre nonlinearity coefficient γ = 1.3 $W^{-1}km^{-1}$ and chromatic dispersion coefficient of 16.7 $ps\cdot nm^{-1}km^{-1}$ is considered.

Span length are 80 km and 50 km which yields 17.6 dB and 11 dB loss per span respectively. Noise figure for all EDFAs is assumed to be 5 dB. A point-to-point transmission with 23 spans is assumed. We first fix the signal transmission PSD to be 21.2 mW/THz and span length to be 80 km. The SNR of central frequency slot which suffers the most NLI and edge frequency slot with the least NLI are shown in Fig. 2 (a) and (b). Then the signal PSD is varied from 21.2 mW/THz to 15 mW/THz, the SNR results of using the hybrid NLI model comparing with exact NLI for both central slot and edge slot are depicted in Fig. 2 (c) and (d). We further vary the span length to 50 km. Fig. 2 (e) and (f) present the SNR of two slots using the proposed method and exact NLI for this case.

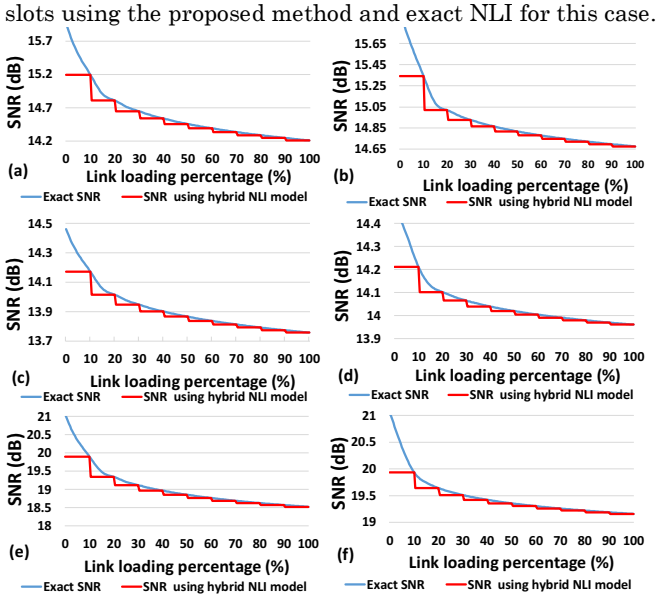

Fig. 2: SNR estimation versus link loading percentage. (a) PSD = 21.2 mW/THz, span length 80km, central slot; (b) PSD = 21.2 mW/THz, span length 80km, edge slot; (c) PSD = 15 mW/THz, span length 80km, central slot; (d) PSD = 15 mW/THz, span length 80km, edge slot; (e) PSD = 15 mW/THz, span length 50km, central slot; (f) PSD = 15 mW/THz, span length 50km, edge slot;

From Fig. 2, it can be observed that the proposed hybrid NLI model can effectively approximate the real performance when the link loading exceeds 100 GHz for various signal PSDs and span lengths. Apart from fixed signal PSD, we also investigate the dynamic signal PSD of each link based on the link loading state. The signal PSD calculated according to (7) for different link loading states is shown in TABLE I. The optimal signal PSD decreases as the loading state increases.

TABLE I

ls	1	2	3	4	5
PSD (mW/THz)	28.99	24.97	23.77	23.05	22.55
ls	6	7	8	9	10
PSD (mW/THz)	22.18	21.88	21.63	21.42	21.24

Fig. 3 demonstrates the SNR performance of the hybrid NLI model with span length of 80 km using the fixed optimal signal PSD = 21.24 mW/THz as mentioned above, compared with flexible signal PSD according to TABLE I. From the figure, we can observe the SNR improvement with flexible optimal signal PSD according to link loading condition over the fixed signal PSD while the edge frequency slot benefits more improvement than the central frequency slot. In the following section, we present the RMSA algorithms using the proposed hybrid NLI model as the tool to evaluate the lightpath performance.

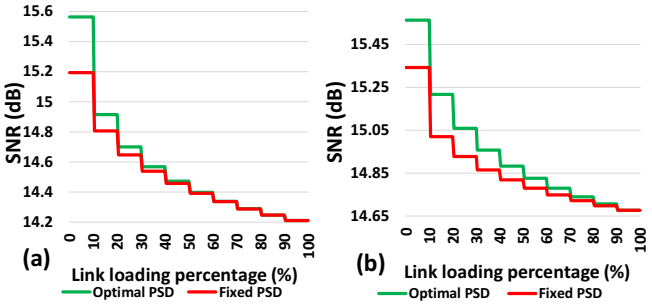

Fig. 3: SNR performance comparison of the proposed hybrid nonlinearity model using fixed PSD = 21.24 mW/THz with using flexible optimal signal PSD. (a) central slot; (b) edge slot

IV. Heuristic Algorithms

In this section, we present several RMSA schemes in EON with the hybrid NLI model described in the previous section. The available modulation formats consist of DP-BPSK, DP-QPSK, DP-8QAM and DP-16QAM. The set of traffic requests is denoted by $\boldsymbol{R}$, where each request $\boldsymbol{r_n} \in \boldsymbol{R}$ is modelled as a triplet (s_n, d_n, T_n). s_n and d_n present the source and destination of the connection request respectively while T_n is the bit rate demand. Since we consider the DP optical system, each polarisation mode carries the same amount of traffic. In this case, the number of frequency slots required with Nyquist shaping to support request T_n using modulation scheme m is shown as:

$$B_{n.m}^{FS} = \left\lceil \frac{T_n}{2 \cdot m \cdot b} \right\rceil \tag{10}$$

where $B_{n.m}^{FS}$ is the number of frequency slots for request n using modulation format m and m = 1 denotes DP-BPSK, 2 denotes DP-QPSK and so on. For each request $\boldsymbol{r_n}$, K least congested paths are calculated between the source and the destination of the request where the weight of each link is calculated as:

$$W_l = \sum_{n,f} PR_{l,f}^{n} / F \tag{11}$$

where $PR_{l,f}^{n} = 1$ if connection n use link l and frequency slot f, 0 otherwise. For each candidate path, we first search for the first-fit continuous and contiguous $B_{n,m}^{FS}$ slots along the candidate path assuming the highest format m=M. In this case, the loading states of the links are updated temporarily given that $B_{n,m}^{FS}$ slots are temporarily allocated. Then we determine NLI by searching the NLI lookup table using the updated loading states of the links and the index of $B_{n,m}^{FS}$ slots. The SNR of the request is computed according to (1) with corresponding ASE and NLI along the candidate path. If the SNR meets the SNR requirement for selected modulation format m, we calculate the cost of the candidate path using (11). If the SNR requirement cannot be satisfied, we set $m = m - 1$, $Cost_{n,k} = inf$ (infinity) and repeat above process for a path until one of the following three criteria is satisfied: 1) RMSA solution feasible for the path k; 2) no slots available for all applicable modulation formats. After calculating all the paths, the algorithm selects the path with minimum cost. The cost of each candidate path is shown as:

$$Cost_{n,k} = NL_{n,k} \cdot NSS_{n,k} \tag{12}$$

where $NL_{n,k}$ and $NSS_{n,k}$ is the number of links and number of required frequency slots respectively of path k for request n. Equation (12) calculates the total number of allocated

frequency slots along all the candidate paths hence selecting the path with minimum cost leads to higher spectrum utilisation.

HM: Heuristic Algorithm Main

1. Set all the links loading states to 1;
2. **for** each traffic request r_n
3. Find K least congested paths $Path_{n,k}$ from source to destination;
4. **for** each candidate path
5. Set $m = M$;
6. **do{**
7. Find first-fit $B_{n,m}^{FS}$ slots along the path;
8. Temporally update link loading states assuming $B_{n,m}^{FS}$ slots being allocated;
9. Determine the NLI according to NLI lookup table;
10. Calculate the SNR of the request r_n according to (1);
11. **if** $SNR \geq SNR_m$
12. Calculate the cost of $Path_{n,k}$ according to (12);
13. **else** $m = m$ - 1; $Cost_{n,k} = inf$;
14. **end if }**
15. **while** ($Cost_{n,k}$ is infinity & $m \neq 0$)
16. **end for**
17. Choose the minimum cost path;
18. **if** any loading state changes
19. Invoke **SNR Checking Function**;
20. **if** no request blocked
21. Accept the request r_n;
22. **else** invoke **service reconfiguration function**;
23. **if** reconfiguration successful
24. Accept the request r_n;
25. **else** block the request r_n;
26. **end if**
27. **end if**
28. **else**
29. Accept the request r_n;
30. **end if**
31. **end for**

The algorithm considers the effects of new requests on established lightpaths. If the loading state of link increases due to the provisioning of a new lightpath, we use the updated NLI with increased loading state of the link for SNR calculation of the new lightpath. Similarly, we re-evaluate the QoT of the established lightpaths sharing the same links using an **SNR Checking Function** with updated loading states of the links. The function returns *request blocked* if the SNR of any established lightpaths drop below the SNR threshold for assigned modulation format (regarded as blocked). In this case, the **Heuristic Algorithm Main** invokes the **Service Reconfiguration Function** to reconfigure all blocked requests. In this paper, we proposed 3 service reconfiguration schemes: 1) a MILP based service reconfiguration; 2) a MILP based heuristic service reconfiguration method; 3) a complete heuristic service reconfiguration scheme.

SNR Checking Function

1. **for** all embedded traffic requests utilizing links with rising loading states
2. Calculate the new SNR according to the new link loading states;
3. **if** new SNR is less than SNR threshold for assigned modulation format
4. **return** (*request blocked*);
5. **end if**
6. **end for**
7. **return** (*no request blocked*);

A. MILP Service Reconfiguration

In case of inter-channel blocking, the MILP based service reconfiguration method reconfigures all the existing connections and new connection request at once. To limit the size of MILP problem, we calculate K-shortest paths for each request in advance. TABLE II lists the size and TABLE III lists the input parameters of the MILP model, while TABLE IV explains the decision variables. The details of the MILP model are described as follows.

TABLE II
Constants

Symbol	Meaning
N	Number of the requests
L	Number of the links
F	Number of the frequency slots
M	Number of the modulation formats
LS	Number of the loading states
K	Number of the shortest path

The objective function (13) is to minimize the highest allocated frequency slot index of the whole network. In this case, the highest link loading state is minimized, which leads to reduced NLI estimation as well as better load balancing of the traffic. Furthermore, it also leaves more available capacity for the future requests with more availability of continuous and contiguous frequency slots in the network.

TABLE III
INPUT PARAMETERS

Symbol	Meaning
$G_{ASE} \in \mathbb{R} > 0$	Per span power spectrum density of ASE noise
$G_{sig} \in \mathbb{R} > 0$	Signal PSD launched into the fibre
$b \in \mathbb{R} > 0$	Bandwidth of each frequency slot
$\mu \in \mathbb{N} > 0$	A very large number (~ 10^4)
$P_{n,k,l} \in \mathbb{B} = \{0,1\}$	Pre-calculated K paths, $P_{n,k,l} = 1$ if k_{th} path of connection n uses link l
$SP_l \in \mathbb{N}$	The number of fibre spans of link l
$SNR_m \in \mathbb{R} > 0$	SNR threshold for modulation scheme m
$T_n \in \mathbb{R} > 0$	Bit rate request of connection n
$B_{n,m}^{FS} \in \mathbb{N}$	Number of frequency slots required for connection n when assigned modulation scheme is m
$G_{NLI}^{ls,f} \in \mathbb{R} > 0$	Per span NLI PSD of frequency slot f for a link of loading state ls (NLI lookup table)

Constraint (13.1) ensures the maximum slot index of each link does not exceed the maximum slot index of the network. Constraint (13.2) ensures that every connection will be accommodated. Due to constraints (13.3) – (13.6), only one path, one modulation format is permitted for each request. Constraint (13.7) ensures non-overlapping of the spectrum for all connections that share the same optical links. Constraint (13.8) ensures that the number of frequency slots allocated to the connection satisfies its bit-rate request. Constraint (13.9) and (13.10) determine the lowest and highest slot index allocated to each connection respectively. Constraint (13.11) is required to satisfy the spectrum contiguity constraint for each connection. Constraint (13.12) determines the spectrum resource pool of each fibre link and constraint (13.13) determines the allocated frequency slot index of each link. Constraint (13.14) – (13.18) determine the maximum slot index MF_l of the link when $\sum_f d_{l,f} = 1$. MF_l equals to zero if no slot is allocated in the link l. Constraint (13.19) ensures each link of one loading state. Constraints

Objective:

$$\text{Minimize } MF\_max \tag{13}$$

Subject to:

$$MF\_max \geq MF_l, \forall\, l \tag{13.1}$$

$$\sum_{k,m,f} x^n_{k,m,f} \geq 1, \forall\, n \tag{13.2}$$

$$\sum_{k,m} z^n_{k,m} = 1, \forall\, n \tag{13.3}$$

$$z^n_{k,m} \geq \Big(\sum_f x^n_{k,m,f}\Big)/\,\mu, \forall\, n, k, m \tag{13.4}$$

$$\sum_m Mod_{n,m} = 1, \forall n \tag{13.5}$$

$$Mod_{n,m} = \sum_k z^n_{k,m}, \forall\, n,m \tag{13.6}$$

$$\sum_{k,m,n} x^n_{k,m,f} \cdot P_{n,k,l} \leq 1, \forall\, l,f \tag{13.7}$$

$$\sum_{k,m,f} x^n_{k,m,f} = \sum_m (Mod_{n,m} \cdot B^{FS}_{n,m}), \forall\, n \tag{13.8}$$

$$FS^n_{min} \leq \mu \cdot \left(1 - \sum_{k,m} x^n_{k,m,f}\right) + f, \forall\, n, f \tag{13.9}$$

$$FS^n_{max} \geq f \cdot \sum_{k,m} x^n_{k,m,f}, \forall\, n, f \tag{13.10}$$

$$FS^n_{max} - FS^n_{min} + 1 = \sum_m (Mod_{n,m} \cdot B^{FS}_{n,m}), \forall\, n \tag{13.11}$$

$$PR^n_{l,f} = \sum_{k,m} (x^n_{k,m,f} \cdot P_{n,k,l}), \forall\, n, l, f \tag{13.12}$$

$$H_{l,f} = \sum_n PR^n_{l,f} \cdot f, \forall\, l, f \tag{13.13}$$

$$MF_l \geq H_{l,f}, \forall\, l, f \tag{13.14}$$

$$MF_l \leq H_{l,f} + \mu \cdot (1 - d_{l,f}), \forall\, l, f \tag{13.15}$$

$$\sum_f d_{l,f} \leq 1, \forall\, l \tag{13.16}$$

$$MF_l \geq 0, \forall\, l \tag{13.17}$$

$$MF_l \leq \mu \cdot \sum_f d_{l,f}, \forall\, l \tag{13.18}$$

$$\sum_{ls} y_{ls,l} = 1, \forall\, l \tag{13.19}$$

$$\sum_{ls} (y_{ls,l} \cdot ls) \geq MF_l \cdot \frac{LS}{F} + 1/mu, \forall\, l \tag{13.20}$$

$$\sum_{ls} (y_{ls,l} \cdot ls) \leq MF_l \cdot \frac{LS}{F} + 1 + 1/mu, \forall\, l \tag{13.21}$$

$$G_{sig} \sum_m \frac{Mod_{n,m}}{SNR_m} \geq G_{ASE} \sum_l \left(PR^n_{l,f} \cdot SP_l\right) + \sum_l (E^{n,l}_{NLI} \cdot SP_l), \forall\, n, f \tag{13.22}$$

$$E^{n,l}_{NLI} \geq \mu \cdot \left(PR^n_{l,f} - 1\right) + \sum_{ls} \left(y_{ls,l} \cdot G^{ls,f}_{NLI}\right), \forall\, n, f, l \tag{13.23}$$

(13.20) and (13.21) determine the loading states of the links according to their highest allocated slot indexes. For unused links, the loading states of the links remain to be minimum. Constraint (13.22) ensures SNR requirement is satisfied for assigned modulation format taking ASE and NLI into account. Constraint (13.23) determines the NLI PSD of each connection using hybrid NLI model. The NLI of a request in this case depends on allocated path, loading states of the links along the path and the index of assigned frequency slot.

The above MILP problem is solved first to minimize the highest allocated slot index in the network. Given the minimum *MF_max* value $\boldsymbol{a}$, the MILP model is again solved for the secondary objective with previous constraints (13.1) – (13.23) and a new constraint (14.2) to ensure the *MF_max* being minimum. In this case, the objective is to minimize the total number of allocated slots in the network As a result, the number of available frequency slots is maximized.

Objective:

$$\text{Minimize } \sum_{n,l,f} PR^n_{l,f} \tag{14}$$

Subject to:

$$\text{Constraint (14.1) – (14.23)} \tag{14.1}$$

$$MF\_max = a \tag{14.2}$$

TABLE IV
DECISION VARIABLES

Symbol	Meaning
$x^n_{k,m,f} \in \mathbb{B}$	$x^n_{k,m,f} = 1$ if frequency slot f, modulation format m and k_{th} path is assigned to connection n, 0 otherwise
$z^n_{k,m} \in \mathbb{B}$	$z^n_{k,m} = 1$ if modulation format m and k_{th} path is assigned to connection n, 0 otherwise
$Mod_{n,m} \in \mathbb{B}$	$Mod_{n,m} = 1$ if connection n utilizes modulation format m, 0 otherwise
$y_{ls,l} \in \mathbb{B}$	$y_{ls,l} = 1$ if link l is within ls loading state, 0 otherwise
$PR^n_{l,f} \in \mathbb{B}$	$PR^n_{l,f} = 1$ if connection n use link l and frequency slot f, 0 otherwise
$d_{l,f} \in \mathbb{B}$	$d_{l,f} = 1$ if frequency slot f is the maximum frequency slot index allocated in link l, 0 otherwise
$H_{l,f} \in \mathbb{N}$	$H_{l,f} = f$ if f is occupied for link l, 0 otherwise
$FS^n_{min} \in \mathbb{N}$	The minimum assigned frequency slot index of connection n
$FS^n_{max} \in \mathbb{N}$	The maximum assigned frequency slot index of connection n
$MF_l \in \mathbb{N}$	Maximum frequency slot index of link l
$E^{n,l}_{NLI} \in \mathbb{R} \geq 0$	Nonlinearity PSD per span in link l of connection n
$MF\_max \in \mathbb{N}$	The maximum frequency slot index of all the link

B. MILP based Heuristic Service Reconfiguration

The MILP formulation proposed previously is an NP complete problem [6], [31]. Hence, it is challenging to solve the MILP model in real time for reasonably large networks and a large number of traffic requests. Therefore, to provide the RMSA reconfiguration solution for a large number of requests in large-scale networks, we propose a MILP based heuristic algorithms to reconfigure connections in a series of groups of requests. We apply the request reordering policy to the MILP based heuristic, described as **shortest path first**. The traffic requests are reordered in the descending order of their shortest paths. For the requests of the same shortest path length, we reorder them in the descending order of their bit rate demands. The traffic demand with the shortest path and highest bit rate demand is served first.

For the MILP based heuristic service reconfiguration algorithm, we divide the traffic requests into several small subsets, with each subset A consisting of S requests, except the last subset with size (N mod S) according to the request reordering policy mentioned above. To provision traffic request subset A_c, we denote A_{pre} as the collection of previous subsets ($A_1 \ldots A_{c-1}$) that are already provisioned in the network. The MILP based heuristic provisions each request subset one by one by solving the subset MILP formulation shown in (15) – (15.3). The input parameters and the decision variables of sub MILP problem are the same as listed in TABLE II, III and IV. Most of the constraints are similar to constraints (13.1) – (13.23). Hence, we make the modification of the constraints (13.1) – (13.23) to form the constraints for

the subset MILP formulation. For constraints (13.2) – (13.6) and (13.8) – (13.12), we apply $\forall\, n \in A_c$ instead of original range $\forall\, n$. This ensures that the only traffic requests in subset A_c will be accommodated. For constraints (13.7), (13.22) and (13.23), the range of request n is replaced by $n \in A_{pre} \cup A_c$. The modified constraint (13.7) ensures the allocated slots of current subset A_c do not overlap with the spectrum used by previously provisioned subset A_{pre}. The modified constraint (13.22) and (13.23) ensure SNR requirements are met for both current subset A_c and previous subset A_{pre}. Apart from modified constraints, two more constraints (15.2) and (15.3) are added for the subset MILP formulation. The constant $X\_Input^{n}_{k,m,f}$ in (15.2) is the RMSA solution from previous request subset A_{pre}. Constraint (15.2) guarantees that the decision variable $x^{n}_{k,m,f}$ of the current subset is equivalent to the previous solution for the requests from A_{pre}. $Y\_Input_{ls,l}$ in (15.3) is the pre-estimated loading state of each link in the main MILP based heuristic algorithm. It is a Boolean parameter equaling to 1 when link l is estimated of loading state ls; 0 otherwise. $Y\_Input_{ls,l}$ is input parameter for the sub MILP while the constraint (15.3) ensures that the actual loading states in sub MILP do not exceed the pre-estimated loading states $Y\_Input_{ls,l}$.

Objective:

$$\text{Minimize}\ \ \beta \cdot \sum_l MF_l + (1-\beta)\sum_{n,l,f} PR^{n}_{l,f}\ ,n \in A_{pre} \cup A_c \qquad (15)$$

Subject to:

$$\text{Modified constraints of (13.1) – (13.23)} \qquad (15.1)$$

$$x^{n}_{k,m,f} = X\_Input^{n}_{k,m,f}, \forall\, n \in A_{pre}, k, m, f \qquad (15.2)$$

$$\sum_{ls}\left(y_{ls,l} * ls\right) \le \sum_{ls}\left(Y\_Input_{ls,l} * ls\right), \forall\, l \qquad (15.3)$$

The objective function (15) of sub MILP problem includes minimizing several targets. When the weight factor $\beta = 0$, the objective is to minimize the overall number of allocated frequency slots. The objective aims to minimize the summation of maximum frequency slot index assigned to each link when $\beta = 1$. For $0 < \beta < 1$, both features are minimized with the weight β.

As $Y\_Input_{ls,l}$ is pre-estimated loading states of all the links in the network, the actual loading states of the links of solving the RMSA problem cannot exceed the pre-estimated values, as shown in constraint (15.3). When the pre-defined loading states $Y\_Input_{ls,l}$ are too large. Higher NLI is assigned, causing severe NLI overestimation. On the other hand, when pre-estimated links loading states $Y\_Input_{ls,l}$ are too small, there is infeasible RMSA solution of links in such low loading condition to serve all the traffic. According to this principle, the proposed MILP based heuristic reconfiguration scheme aims to yield a proper pre-estimated $Y\_Input_{ls,l}$ to provision all the request subsets as well as to minimize the two features mentioned in the sub MILP earlier. Initially, the pre-estimated loading states of the links is set to 1 for every link, as shown in line 2. We then dynamically adjust the estimated $Y\_Input_{ls,l}$ according to the request subsets. For each request subset A_c consisting of a set of bit rate demands, the algorithm invokes the sub MILP solver to solve the problem in (15) – (15.3) to obtain the RMSA solution. Line 4 – 7 shows that when a solution is found, the RMSA result $x^{n}_{k,m,f}$ is recorded and we set $X\_Input^{n}_{k,m,f} = x^{n}_{k,m,f}$ as the input parameter for the following request subset. The input $X\_Input^{n}_{k,m,f}$ enables the constraint (15.2) to ensure that the consistency of RMSA solution of previous request subsets.

PH1: MILP based Heuristic Service Reconfiguration

1. Reorder the connection requests according to reordering policy;
2. Initialize all the loading states by setting $\sum_{ls}\left(Y\_Input_{ls,l} \cdot ls\right) = 1\ \forall\, l$;
3. **for** each request subset A_c, c = 1, 2, 3, …, $\lceil N/S \rceil$
4. Solve the subset MILP formulation in (15) – (15.3);
5. **if** a solution is found
6. Accept the request subset;
7. Record the RMSA solution $X\_Input^{n}_{k,m,f} = x^{n}_{k,m,f}$;
8. **if** $c_{ug} \neq \emptyset$ & $c == c_{ug}$
9. Recalculate $Y\_Input_{ls,l}$ according to RMSA solution $x^{n}_{k,m,f}$;
10. Set $c_{ug} = \emptyset$;
11. **end if**
12. $c = c + 1$;
13. **else**
14. **if** $Y\_Input_{LS,l} == 1\ \forall\, l \in$ candidate paths in A_c
15. Upgrade $Y\_Input_{ls,l}$ to next level $\forall\, l \notin$ candidate paths in A_c;
16. **else**
17. Upgrade $Y\_Input_{ls,l}$ to next level $\forall\, l \in$ candidate paths in A_c;
18. Record c by $c_{ug} = c$;
19. Set $c = 1$;
20. Jump to step 3;
21. **end if**
22. **end if**
23. **end for**

The sub-MILP solver may not provide the results as the maximum allocated slot index exceeds the bounds of $Y\_Input_{ls,l}$, resulting in failure of complying with the constraint (15.3). In this case, the pre-estimated loading states need to be upgraded to satisfy constraint (15.3). Since there is no knowledge about which paths to be selected from the candidate set, we upgrade the loading states of all the links of all the candidate paths in the subset A_c to the next level ($ls = ls + 1$, for all associated links), as shown in line 16 – 17. Line 18 shows the request subset index c is recorded as c_{ug} when the upgrade occurs. Then we reset c = 1 to repeat the algorithm from first request subset with updated $Y\_Input_{ls,l}$ until $c == c_{ug}$, as shown in line 8. We also consider the situation where the MILP solver gives different RMSA results using updated $Y\_Input_{ls,l}$. In this case, the RMSA solution might be again beyond the boundary of updated $Y\_Input_{ls,l}$. In this case, we keep upgrading $Y\_Input_{ls,l}$ of the rest links to next level until subsets A_1 … A_{cug} are completely provisioned as shown in line 14 – 15. Line 9 – 10 shows that after successfully provisioning subset A_1 … A_{cug}, we calculate $Y\_Input_{ls,l}$ according to the RMSA results and set c_{ug} as the empty set. The process is repeated until the $Y\_Input_{ls,l}$ is found to accommodate all the request subsets.

C. Heuristic Service Reconfiguration

To further reduce the complexity of service reconfiguration, a complete heuristic service reconfiguration scheme is proposed. Unlike previous MILP based reconfigurations, the complete heuristic reconfiguration function only reconfigures the blocked traffic requests. It works similar to the main algorithm by using K least congested paths. It starts searching from the highest modulation format and assigning the first-fit spectrum. The details of the heuristic service reconfiguration function are shown in the pseudo code below, shown as **PH2**. The service

reconfiguration function stops searching for the modulation spectrum combination for a candidate path when allocating spectrum leads to further blocking of the requests. This strategy prevents reconfiguration loops where the reconfiguration function triggers further reconfigurations. This reduces the overall complexity of the algorithm. If all candidate paths fail, the function returns *reconfiguration failure* to the main reconfiguration. The function returns *reconfiguration success* only when all blocked requests are reconfigured successfully. The new lightpath will not be permanently established unless all blocked requests are successfully reconfigured.

PH2: Heuristic Service Reconfiguration Function

```
1.  Reorder the blocked traffic request based on reordering policy;
2.  for blocked traffic request 1, …
3.    Find K least congested paths;
4.    for each candidate path
5.      for m = M; m >1; m – –;
6.        Search for first-fit B^FS_{n,m} slots;
7.        Temporally update loading states of the links;
8.        if any loading state changes
9.          if any existing request blocked
10.           Set cost of the path to be infinity;
11.           break for;
12.         else
13.           Calculate the SNR of the blocked request;
14.           if SNR ≥ SNR_m
15.             Calculate the cost of the path according to (12);
16.             break for;
17.           end if
18.         end if
19.       else repeat step 13 – 17;
20.       end if
21.     end for
22.   end for
23.   if any cost of the K paths not equal to infinity
24.     Choose the path with minimum cost;
25.     Temporally accept the reconfigured lightpath;
26.     Temporally release previously allocated resource;
27.   else
28.     return (service reconfiguration failure);
29.   end if
30. end for
31. Accept service reconfiguration;
32. return (service reconfiguration success);
```

V. Performance Results

In this section, we explain the evaluation of our proposed solutions based on an extensive simulation study. We first describe the simulation setup and then present the results for the proposed algorithms in incremental traffic requests sequentially loaded EON.

A. Simulation Environment Setup and Benchmark

We evaluate the performance of our proposed approaches in two network topologies to validate their effectiveness in both small network and large network: 1) a small network with 6 nodes and 9 links (N6S9); 2) national science foundation (NSF) network with 14 nodes 21 links, as shown in Fig. 4. Each optical link is of bi-directional using a pair of fibres. We consider that the network operates in the C-band of 193.6 THz and frequency slot bandwidth b = 12.5 GHz. Total bandwidth B is 4 THz, thus the number of slots F equals to 320. M is 4 corresponding to four modulation levels while the number of shortest paths per connection, K = 3 for the main RMSA algorithm and the service reconfiguration algorithms. The spectra window size of the proposed hybrid NLI model is 100 GHz and 200 GHz, hence the number of loading states LS corresponds to 20 and 40 for comparison. The same parameters of fibre and EDFA described in section III are used. Pre-FEC bit error rate (BER) requirement of all the traffic requests is set to 4 x 10^{-3}. The SNR threshold for each modulation format to achieve the pre-FEC BER target is calculated which is 5.46 dB for DP-BPSK, 8.47 dB for DP-QPSK, 12.45 dB for DP-8QAM and 15.13 dB for DP-16QAM. For the proposed MILP based heuristic service reconfiguration, the subset size S is set to be 2 and weight factor β is 0.5. We evaluate two types of traffic requests for the simulation: low-to-medium bandwidth requests that are uniformly distributed between 40 Gbps and 400 Gbps and medium-to-high bandwidth requests that are uniformly distributed between 100 Gbps and 600 Gbps.

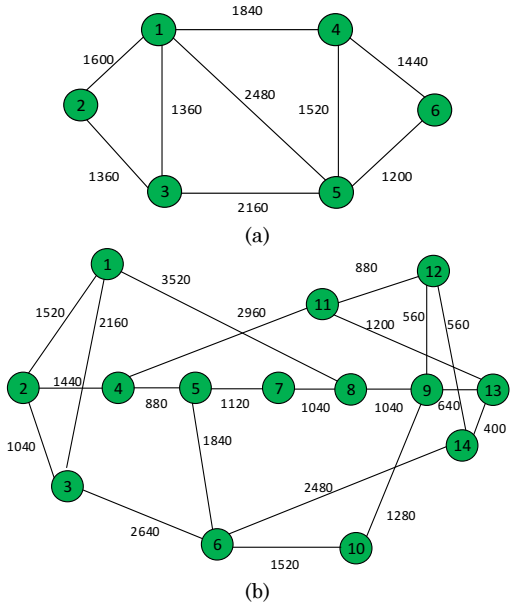

Fig. 4. Network topologies (unit: km). (a) N6S9 topology; (b) NSF topology.

To evaluate the performance of the proposed resource allocation algorithm with different service reconfiguration schemes, we use the ILP method and the sequential RMSA heuristic algorithm described in [6] as the benchmark. The benchmark method adopts the maximum transmission distance method with a guard band for modulation level assignment to model the impact of the physical layer impairments. The maximum permitted distance is different for each modulation level m. For higher modulation level, the reach distance is shorter while the reach distance increases with lower modulation formats. The benchmark method pre-calculates K shortest paths for each pair of source-destination for both ILP and the RMSA heuristic algorithm, while the routing decision is chosen among the K candidate paths. However, it only indicates transmission distance for each modulation format regardless of signal power. If the signal PSD changes, the pre-defined reach distance may no longer support error-free transmission. Therefore, in our approach, we first calculate the worst-case NLI PSD assuming full channel occupancy for different transmission PSDs. The maximum transmission distance of each modulation format is then calculated to achieve pre-set pre-FEC BER for different signal PSDs using (1) with

worst-case NLI. TABLE V shows the longest permitted distance of each modulation format for error-free transmission with fibre parameters described earlier. The guard band for the benchmark is set to 12.5 GHz (one frequency slot) as similar to [6].

We first assess the proposed hybrid nonlinearity model in the network, then the performance of the proposed service reconfiguration algorithms is evaluated against benchmark methods in terms of network utilization and spectrum efficiency. Later, the complete algorithms are also performed for incremental traffic request loaded into NSF network to measure the blocking probability.

TABLE V
REACH DISTANCE (KM)

Signal PSD (mW/THz)	DP-BPSK	DP-QPSK	DP-8QAM	DP-16QAM
10.64	9680	4800	1920	1040
13.40	11600	5760	2240	1200
16.87	13120	6560	2560	1360
21.24	13760	6880	2720	1440
26.73	13040	6480	2560	1360
33.66	10960	5440	2160	1120
42.38	8240	4080	1600	880

B. *Hybrid nonlinearity model assessment in the network*

In this section, to investigate the benefit of the proposed hybrid nonlinearity model (HNM) in the EON, we evaluate the performance of RMSA solution in EON using the proposed HNM against the same RMSA using the worst-case (WC) NLI as the benchmark. The proposed heuristic main algorithm with the complete heuristic reconfiguration (**PH2**) is selected as the evaluated RMSA scheme. For the routing in the proposed RMSA, we slightly modify the routing scheme in the original RMSA algorithm to examine the proposed HNM for different routing strategies. Therefore, *K*-least congested path routing strategy is evaluated along with the shortest-path routing. We load incremental 100 Gbps traffic requests into NSF optical network. *LS* is set 20 for the RMSA scheme using the proposed hybrid nonlinearity model and the signal PSD is 19 mW/THz. As the benchmark method employ the WC NLI as the NLI model, the service reconfiguration will not be triggered in this case. The requests blocking ratio for the proposed RMSA using 2 NLI models with *K*-least congested path routing and shorting-path routing are shown in fig. 5. From the figure, it shows around 5% more requests can be accepted at 1% blocking ratio using the shortest-path routing algorithm. When adopting *K*-least congested routing, 11.5% more traffic requests can be achieved. Apart from the proposed RMSA schemes, the proposed HNM proves to improve the network capacity regardless of the routing strategies while the capacity improvement depends on the RMSA schemes with selected routing algorithm.

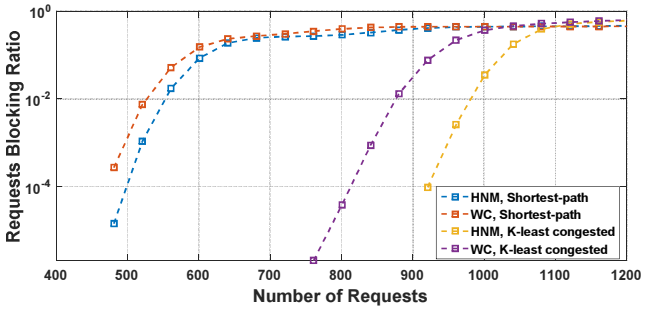

Fig. 5: Blocking ratio for incremental 100 Gbps requests in the NSF network.

C. *Performance comparison of service reconfiguration approaches*

1) *Results for N6S9 network with low-to-medium bandwidth requests*

For the N6S9 network, we evaluate and compare the results of the proposed MILP reconfiguration (referred to as **PM** in this section), the benchmark ILP (**BI**), the proposed MILP based heuristic reconfiguration algorithm (**PH1**) and the proposed complete heuristic service configuration (**PH2**) and the benchmark heuristic (**BH**). Service reconfiguration algorithms have the knowledge of all the existing traffic thus they are regarded as off-line algorithms. To make the comparison of reconfiguration algorithms, the results are averaged over 20 traffic profiles where each traffic profile consists of 20 requests between randomly selected pairs of nodes. The PM and the BI are simulated on a desktop with 3.1 GHz Intel i7-3770s CPU and 16 GB memory using IBM ILOG CPLEX version 12.7.1. The running time for the PM is between 1 minute to 10 minutes for low-to-medium bandwidth requests with proper upper bound and lower bound of the *MF_max*. The running time for *LS* = 40 is 1.5 - 2 times more than the case when *LS* = 20 due to higher MILP complexity. For medium-to-high bandwidth requests, it takes longer to obtain the optimal results compared to low-to-medium bandwidth requests. The time required for the PH1 calculates the RMSA results within 1 minute. In terms of PH2, the RMSA results can be obtained in a few milliseconds.

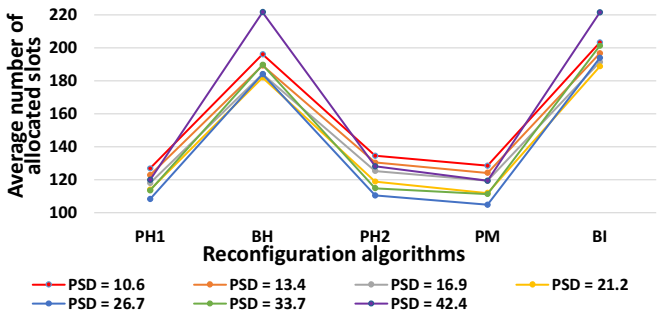

Fig. 6: Average number of allocated slots versus algorithms for different signal PSDs with low-to-medium bandwidth requests.

First, we consider the case where traffic profiles are low-to-medium bandwidth requests. Fig. 6 shows the average number of allocated frequency slots in the network using different algorithms for different PSDs (*LS* = 40 for the proposed algorithms) under low-to-medium bandwidth requests. Although two proposed heuristics require the similar amount of spectrum resources, PH1 allocates 1.7% - 7% fewer number of slots than PH2 for different PSDs. In this case, the PM utilizes the least spectrum resources due to its secondary goal of minimizing the number of allocated frequency slots. The proposed MILP and two heuristics allocate approximate 40% - 45% fewer frequency slots compared to BI and BH when PSD = 21.2 mW/THz. The benefits of the proposed solutions are due to the hybrid NLI model, which makes a less conservative NLI estimation. Thus, the lightpaths can utilize more high modulation formats with accurate NLI information, which is shown in Fig. 7 with two PSDs. In this case, it leaves more free slots in the network for future connection requests. The best PSD

among the options for two benchmark methods is 21.2 mW/THz which maximizes the transmission distance assuming the worst-case NLI. However, the best PSD for the 3 proposed service reconfiguration solutions to achieve minimum spectrum usage is 26.7 mW/THz. This is because less congested link yields less NLI compared to the worst-case NLI. Therefore, PSD of 26.7 mW/THz leads to better SNR performance.

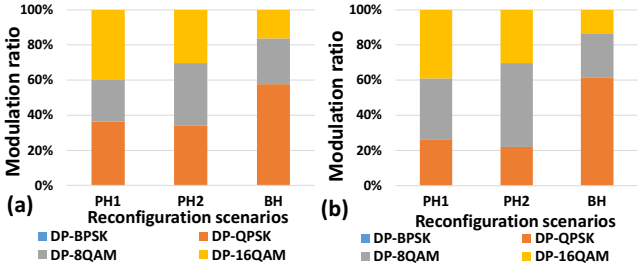

Fig. 7: Modulation format ratio versus different algorithms with low-to-medium bandwidth requests. (a) PSD = 21.2 mW/THz; (b) PSD =26.7 mW/THz

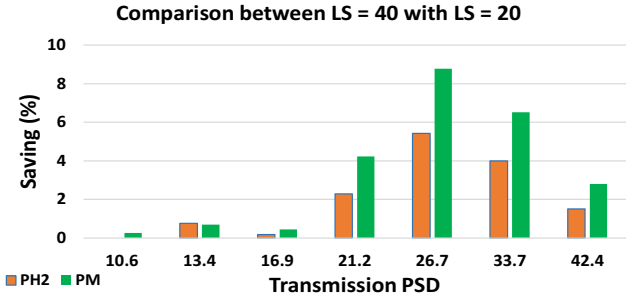

Fig. 8: Allocated slots number saving for LS = 40 over LS = 20 with low-to-medium bandwidth requests.

To understand the effect of spectra window size defined in the proposed hybrid NLI model on the network, we compare the performance of the PM and the PH2 where LS = 40 (window size: 100 GHz) with the case where LS = 20 (window size: 200 GHz) for 4 THz bandwidth. Fig. 8 illustrates the percentage saving on the number of allocated slots for the case with LS = 40 over LS = 20 with low-to-medium bandwidth requests. It shows that the case LS = 40 requires fewer slots than LS = 20 for both PH2 and PM. This is because with smaller spectra windows size defined, the more NLI estimation accuracy can be obtained. The improved NLI accuracy results in less spectrum waste for RMSA solution. On the other hand, the complexity of 3 proposed service reconfiguration solutions grow with the increasing number of the defined link loading states LS.

The parameters β and subset size S defined in PH1 have considerable impact to network performance. In this section, we also vary the subset size S from 2 to 1, the β value from 0.5 to 0 and 1 respectively and compare their performance with the proposed β = 0.5 and S = 2 as shown above. Fig. 9 (a) shows the average maximum allocated slot index *MF_max* against the increasing signal PSDs. As with β = 1, PH1 aims at minimizing the summation of maximum slot index among all the links. Therefore, the combination with S = 2 and β = 1 achieves the minimum *MF_max*. Similarly, PH1 with β = 0 and S = 2 leads to the highest *MF_max* among the tested combinations as its optimisation target is irrelevant to *MF_max*. We also vary the S to 1 and result depicts that S = 2 can yield slightly less *MF_max* compared to the PH1 with S = 1. Fig. 9 (b) shows the average number of allocated slots against the signal PSDs for different S and β. Contrast to the results in Fig. 9 (a), PH1 with β = 0 requires the fewest slots number while β = 1 uses the most spectrum resources. This is because β = 0 of PH1 is to minimize the number of slots assigned in the network. For the case PH1 with subset size S = 1, the algorithm assigns slightly more slots compared to S = 2. The larger subset size of PH1 can achieve better results than smaller subset size in terms of the less maximum slot index and lower number of allocated slots. However, it also needs more time to solve the sub MILP problem, with approximate 1 minute for S = 2 and 20 - 30 seconds for S = 1.

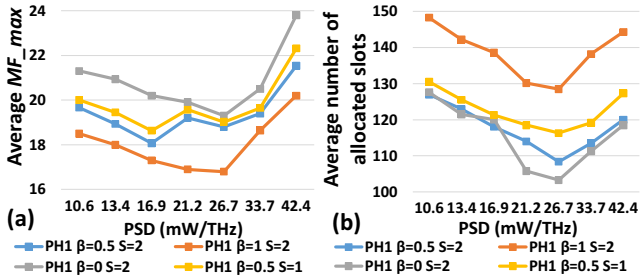

Fig. 9: Performance comparison of PH2 with different subset size S and β. (a) average *MF_max* against the signal PSDs; (b) average number of allocated slots against the signal PSDs.

2) Results for N6S9 network with medium-to-high bandwidth requests

TABLE VI
AVERAGE ALLOCATED SLOTS NUMBER

	PSD 10.6	PSD 13.4	PSD 16.9	PSD 21.2	PSD 26.7	PSD 33.7	PSD 42.4
PH1	198	194	186	180	176	183	192
PH2	206	202	196	189	180	185	198
PM	216	196	198	190	171	194	203
BI	290	286	282	281	289	290	317
BH	288	277	270	262	270	280	335

The important performance metrics such as the average *MF_max*, the number of allocated slots and the modulation format ratio show similar characteristics and trends for medium-to-high bandwidth requests in NSF network compared to low-to-medium bandwidth requests in the N6S9 network. Due to the space constraints, we only presents the average number of allocated frequency slots for PH1, PH2, PM, BI and BH in TABLE VI. Again, the proposed service reconfiguration solutions utilize 40% - 70% fewer frequency slots compared to the benchmark methods. The PH1 approach is observed to use less spectrum resources even compared to PM when PSD ≠ 26.7 mW/THz. This is because the primary objective of PM is only to minimize *MF_max* while the PH1 minimizes both features (summation of *MFl* and the number of allocated frequency slots) with weight β.

3) Results for NSF network of both traffic profiles

We also apply the two traffic requests to the large NSF topology to study how the proposed reconfiguration algorithms perform. The number of traffic requests for each traffic profile is set to 30 for NSF network. The results are calculated and averaged based on 20 traffic profiles. The PM and BI consume a significant amount of time to provide solutions for NSF network due to their complexity of solving MILP (CPLEX aborted after 6-10 hours searching). For large networks, it is infeasible to implement BI or PM approaches for practical timescale. Therefore, in this sub-section, we compare the results of the PH1, PH2 with the BH.

In Fig. 10, we present the number of allocated frequency

slots as a function of PSDs for both traffic scenarios. The curve of BH (brown triangle markers) is associated with left side blue vertical axis and curves of PH1 and PH2 (circle markers) are associated with right side red vertical axis. The PH1 approach saves slightly more slots compared to PH2, due to better resource optimisation of sub-MILP formulation. The PH1 and PH2 can save up to 80% and 70% number of slots for low-to-medium and medium-to-high bandwidth requests respectively compared to BH when the PSD is between 21.2 mW/THz and 26.7 mW/THz. It shows the number of slots saving increases when PSD increases.

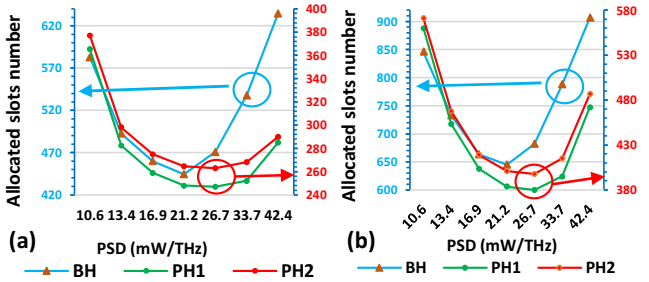

Fig. 10: Average number of allocated slots versus transmission PSD. (a) 40 Gbps – 400 Gbps requests. (b) 100 Gbps – 600 Gbps requests.

D. Performance evaluation of complete proposed RMSA algorithm in incrementally loaded NSF network

To evaluate the performance of the proposed schemes in a realistic scenario with dynamic incremental traffic requests, we incrementally load the NSF network with low-to-medium and medium-to-high bandwidth requests. Considering the space constraint, we choose to show the requests for NSF network other than N6S9 network as it is a more realistic network. The requests are randomly generated following the same traffic distribution described earlier. We evaluate the request blocking ratio and spectrum efficiency of the proposed solutions. The service request blocking probability is expressed as:

$$BP_i = Block_i / i \quad (16)$$

where $Block_i$ is the average number of blocked requests after provisioning i_{th} request. To build statistical results of the service blocking probability and network utilization, the complete RMSA algorithm is repeated **2000** times. Apart from previous benchmark method, we further include the congestion-aware RMSA described in [20] as the second benchmark (**CA-BH2**) in this section. The **CA-BH2** utilizes the congestion-aware routing strategy to choose the least congested routing path with weight of each link as per equation (11). Based on the calculated path, CA-BH2 adopts the first-fit spectrum assignment to allocate resource to the connections. NLI modelling in CA-BH2 considers using the GN model assuming full channel. Details of the NLI model is refer to equation (1) – (3) in [20].

The PM and BI approach cannot provide feasible solution for service reconfiguration due to their complexity for NSF network. As the algorithm is repeated thousands of times, PH1 is not able to give the results in reasonable amount of time. Therefore, we compare the performance of the **proposed heuristic algorithm main** using **PH2** as the service reconfiguration (LS = 40) with the sequential RMSA of the **BH** and **CA-BH2**.

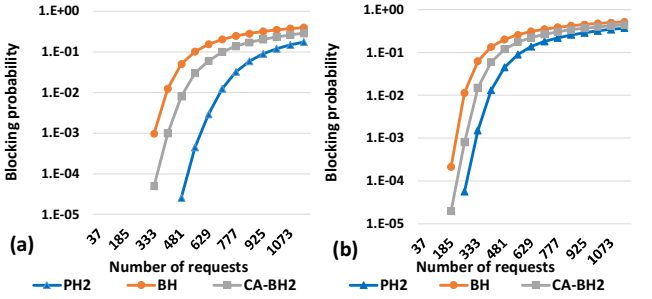

Fig. 11: Blocking probability versus the number of loaded requests when PSD = 19.3 mW/THz. (a) 40 Gbps – 400 Gbps requests; (b) 100 Gbps – 600 Gbps requests.

Fig. 11 shows the requests blocking probability against the number of the requests when PSD = 19.3 mW/THz. The results clearly show that the proposed scheme with PH2 accept approximately 300 and 200 more low-to-medium bandwidth requests at 1% blocking probability compared to the BH and CA-BH2 respectively. Similarly, 148 and 51 more medium-to-high bandwidth requests can be accepted respectively compared to BH and CA-BH2. The average network throughput when the network reaches 1% blocking ratio for two algorithms is shown in Fig. 12. The results indicate that the proposed solution with PH2 as service reconfiguration scheme can serve 25.5 Tbps – 55.7 Tbps more capacity than both benchmark solutions at 1% blocking ratio for low-to-medium bandwidth requests. Similarly, 15.86 Tbps – 42.1 Tbps more network throughput can be achieved using the proposed solution for different PSDs with medium-to-high bandwidth requests.

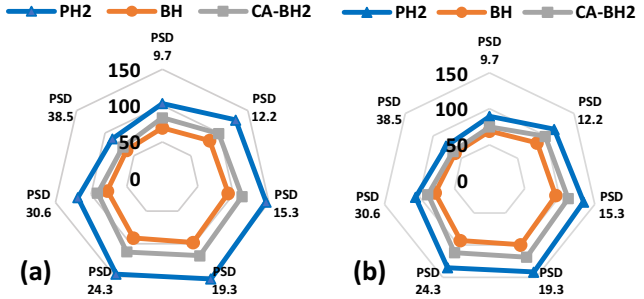

Fig. 12: Network throughput when NSF network reaches 1% blocking probability. (a) 40 Gbps – 400 Gbps requests; (b) 100 Gbps – 600 Gbps requests.

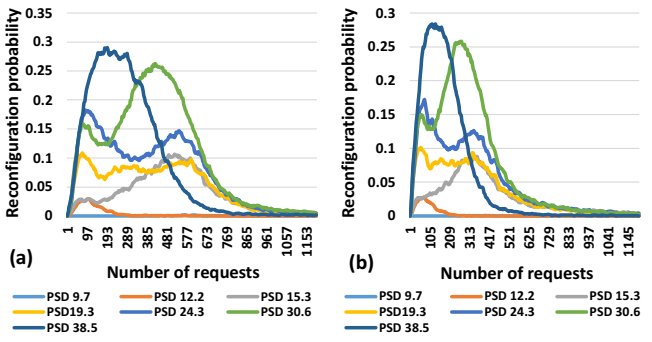

Fig. 13: Service requests reconfiguration probability of PH2 against the increasing number of traffic. (a) 40 Gbps – 400 Gbps requests; (b) 100 Gbps – 600 Gbps requests.

Fig. 13 demonstrates the probability of reconfiguration probability of using PH2 as the reconfiguration scheme against the increasing number of loaded traffic for both

traffic profiles. Both Fig.12 (a) and (b) show that the network requires more reconfiguration as the signal PSD increase. This is obvious as the network operate in high NLI regime, making the NLI the dominant noise. Therefore, the NLI effect on the signal QoT is stronger than the low signal PSD, due to more SNR degradation with increasing link load. In table VII, we list the number of service reconfiguration required when 800 incremental requests loaded into the NSF network for different signal PSDs and both traffic patterns. Similar to the results in Fig. 13, the number of service reconfiguration increases as the signal PSD raises. However, fewer number of reconfigurations are executed for PSD = 38.5 mW/THz compared to PSD = 30.6 mW/THz. This happens as the network in high NLI regime with PSD = 38.5 mW/THz suffers from higher blocking probability than the network with PSD = 30.6 mW/THz. As a result, fewer number of requests can be accepted for PSD 38.5 mW/THz compared to PSD = 30.6 mW/THz, making the overall reconfiguration number smaller. The high NLI also makes successful reconfiguration more difficult than low NLI.

TABLE VII
AVERAGE SERVICE RECONFIGURATION NUMBER WITH PH2 FOR 800 REQUESTS

Signal PSD (mW/THz)	9.7	12.2	15.3	19.3	24.3	30.6	38.5
Low-to-medium traffic	0.07	1.3	17	21	33	53	45
Medium-to-large traffic	0.02	1	12	14	21	34	26

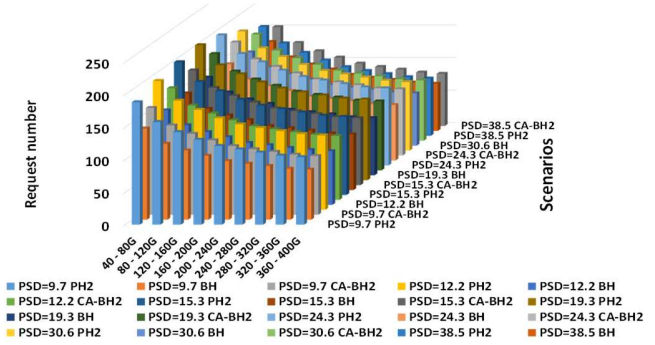

Fig. 14: Bit-rate distribution of accepted requests for low-to-medium bandwidth traffic requests.

Fig. 14 presents the average bit-rate distribution of all accepted low-to-medium bandwidth requests. When PSD = 19.3 mW/THz, the proposed solution accepts approximately 40% and 16.3% more different bit-rate requests compared to BH and CA-BH2 respectively. The graph also implies small bit-rate requests have better acceptance ratio than the large bit-rate request. The case of the medium-to-high bandwidth traffic also shows the similar trend regarding the bit-rate distribution of accepted request. Therefore, we do not show the results due to limitation of space.

VI. CONCLUSION

In this paper, we have proposed a novel hybrid nonlinearity estimation model for resource allocation in elastic optical networks. The proposed load-aware nonlinearity model provides increased accuracy compared to existing SNR margin method used in maximum transmission distance solutions. It is also significantly simpler in terms of computational complexity as compared to using the accurate nonlinearity model. Based on the proposed hybrid NLI model, we further proposed a complete algorithm with 3 service reconfiguration schemes to solve the RMSA problem in EON. The results show that compared to the benchmark methods, the proposed solutions are able to save a significant amount of spectrum resource, achieve better spectrum efficiency, provide lower blocking probability and higher network capacity with different signal PSDs in our evaluation of two types of networks. The results also indicate that to achieve minimum spectrum usage, the optimal PSD of the proposed solutions decreases as the amount of network traffic increases.

REFERENCES

[1] O. Gerstel, M. Jinno, A. Lord, and S. B. Yoo, "Elastic optical networking: A new dawn for the optical layer?," *Commun. Mag. IEEE*, vol. 50, no. 2, pp. s12–s20, 2012.

[2] A. Gumaste and T. Antony, *DWDM network designs and engineering solutions*. Indianapolis, IN: Cisco Press, 2003.

[3] Y. Pointurier, "Design of low-margin optical networks," in *2016 Optical Fiber Communications Conference and Exhibition (OFC)*, 2016, pp. 1–3.

[4] Y. Pointurier, "Design of low-margin optical networks," *IEEEOSA J. Opt. Commun. Netw.*, vol. 9, no. 1, pp. A9–A17, Jan. 2017.

[5] M. Jinno, H. Takara, B. Kozicki, Y. Tsukishima, Y. Sone, and S. Matsuoka, "Spectrum-efficient and scalable elastic optical path network: architecture, benefits, and enabling technologies," *IEEE Commun. Mag.*, vol. 47, no. 11, pp. 66–73, Nov. 2009.

[6] K. Christodoulopoulos, I. Tomkos, and E. A. Varvarigos, "Elastic Bandwidth Allocation in Flexible OFDM-Based Optical Networks," *J. Light. Technol.*, vol. 29, no. 9, pp. 1354–1366, May 2011.

[7] X. Wan, N. Hua, and X. Zheng, "Dynamic routing and spectrum assignment in spectrum-flexible transparent optical networks," *IEEEOSA J. Opt. Commun. Netw.*, vol. 4, no. 8, pp. 603–613, Aug. 2012.

[8] Z. Zhu, W. Lu, L. Zhang, and N. Ansari, "Dynamic Service Provisioning in Elastic Optical Networks With Hybrid Single-/Multi-Path Routing," *J. Light. Technol.*, vol. 31, no. 1, pp. 15–22, Jan. 2013.

[9] W. Lu and Z. Zhu, "Dynamic Service Provisioning of Advance Reservation Requests in Elastic Optical Networks," *J. Light. Technol.*, vol. 31, no. 10, pp. 1621–1627, May 2013.

[10] X. Wang, M. Brandt-Pearce, and S. Subramaniam, "Impact of wavelength and modulation conversion on translucent elastic optical networks using MILP," *IEEEOSA J. Opt. Commun. Netw.*, vol. 7, no. 7, pp. 644–655, Jul. 2015.

[11] Z. Fan, Y. Li, G. Shen, and C. K. C. Chan, "Distance-Adaptive Spectrum Resource Allocation Using Subtree Scheme for All-Optical Multicasting in Elastic Optical Networks," *J. Light. Technol.*, vol. 35, no. 9, pp. 1460–1468, May 2017.

[12] I. Sartzetakis, K. Christodoulopoulos, C. P. Tsekrekos, D. Syvridis, and E. Varvarigos, "Quality of transmission estimation in WDM and elastic optical networks accounting for space-spectrum dependencies," *IEEEOSA J. Opt. Commun. Netw.*, vol. 8, no. 9, pp. 676–688, Sep. 2016.

[13] Y. Ou, A. Hammad, S. Peng, R. Nejabati, and D. Simeonidou, "Online and offline virtualization of optical transceiver," *IEEEOSA J. Opt. Commun. Netw.*, vol. 7, no. 8, pp. 748–760, Aug. 2015.

[14] P. Poggiolini, "The GN Model of Non-Linear Propagation in Uncompensated Coherent Optical Systems," *J. Light. Technol.*, vol. 30, no. 24, pp. 3857–3879, Dec. 2012.

[15] P. Poggiolini, G. Bosco, A. Carena, V. Curri, Y. Jiang, and F. Forghieri, "The GN-Model of Fiber Non-Linear Propagation and its Applications," *J. Light. Technol.*, vol. 32, no. 4, pp. 694–721, Feb. 2014.

[16] L. Yan, E. Agrell, M. N. Dharmaweera, and H. Wymeersch, "Joint Assignment of Power, Routing, and Spectrum in Static Flexible-Grid Networks," *J. Light. Technol.*, vol. 35, no. 10, pp. 1766–1774, May 2017.

[17] L. Yan, E. Agrell, H. Wymeersch, P. Johannisson, R. Di Taranto, and M. Brandt-Pearce, "Link-Level Resource Allocation for Flexible-Grid Nonlinear Fiber-Optic Communication Systems," *IEEE Photonics Technol. Lett.*, vol. 27, no. 12, pp. 1250–1253, Jun. 2015.

[18] D. J. Ives, P. Bayvel, and S. J. Savory, "Adapting Transmitter Power and Modulation Format to Improve Optical Network Performance Utilizing the Gaussian Noise Model of Nonlinear Impairments," *J. Light. Technol.*, vol. 32, no. 21, pp. 4087–4096, Nov. 2014.

[19] J. Zhao, H. Wymeersch, and E. Agrell, "Nonlinear Impairment-Aware Static Resource Allocation in Elastic Optical Networks," *J. Light. Technol.*, vol. 33, no. 22, pp. 4554–4564, Nov. 2015.

[20] S. J. Savory, "Congestion Aware Routing in Nonlinear Elastic Optical Networks," *IEEE Photonics Technol. Lett.*, vol. 26, no. 10, pp. 1057–1060, May 2014.

[21] P. Poggiolini *et al.*, "The LOGON strategy for low-complexity control plane implementation in new-generation flexible networks," in *Optical Fiber Communication Conference and Exposition and the National Fiber Optic Engineers Conference (OFC/NFOEC), 2013*, 2013, pp. 1–3.

[22] D. J. Ives, A. Lord, P. Wright, and S. J. Savory, "Quantifying the impact of non-linear impairments on blocking load in elastic optical networks," in *Optical Fiber Communications Conference and Exhibition (OFC), 2014*, 2014, pp. 1–3.

[23] R. Wang, S. Bidkar, R. Nejabati, and D. Simeonidou, "Load-aware nonlinearity estimation for efficient resource allocation in elastic optical networks," in *2017 International Conference on Optical Network Design and Modeling (ONDM)*, 2017, pp. 1–6.

[24] A. Carena, V. Curri, G. Bosco, P. Poggiolini, and F. Forghieri, "Modeling of the Impact of Nonlinear Propagation Effects in Uncompensated Optical Coherent Transmission Links," *J. Light. Technol.*, vol. 30, no. 10, pp. 1524–1539, May 2012.

[25] R. Wang, S. Bidkar, R. Nejabati, and D. E. Simeonidou, "Load and Nonlinearity Aware Resource Allocation in Elastic Optical Networks," in *Optical Fiber Communication Conference*, 2017, pp. W1H–5.

[26] A. Yariv, "Signal-to-noise considerations in fiber links with periodic or distributed optical amplification," *Opt. Lett.*, vol. 15, no. 19, pp. 1064–1066, Oct. 1990.

[27] H. Kogelnik and A. Yariv, "Considerations of noise and schemes for its reduction in laser amplifiers," *Proc. IEEE*, vol. 52, no. 2, pp. 165–172, Feb. 1964.

[28] S. P. Singh and N. Singh, "Nonlinear effects in optical fibers: Origin, management and applications," *Prog. Electromagn. Res.*, vol. 73, pp. 249–275, 2007.

[29] A. Rosa, C. Cavdar, S. Carvalho, J. Costa, and L. Wosinska, "Spectrum allocation policy modeling for elastic optical networks," in *High Capacity Optical Networks and Emerging/Enabling Technologies*, 2012, pp. 242–246.

[30] P. Johannisson and E. Agrell, "Modeling of Nonlinear Signal Distortion in Fiber-Optic Networks," *J. Light. Technol.*, vol. 32, no. 23, pp. 4544–4552, Dec. 2014.

[31] I. Chlamtac, A. Ganz, and G. Karmi, "Lightpath communications: an approach to high bandwidth optical WAN's," *IEEE Trans. Commun.*, vol. 40, no. 7, pp. 1171–1182, Jul. 1992.